THE JOURNAL OF PHYSICAL CHEMISTRY B

Article

pubs.acs.org/JPCB

Infrared Probing of Equilibrium and Dynamics of Metal–Selenocyanate Ion Pairs in *N,N*-Dimethylformamide Solutions

Hyewon Son,[†] Haneul Jin,[†] Seung Ryul Choi,[†] Hyun Wook Jung,[‡] and Sungnam Park*[,†,§]

[†]Department of Chemistry, Korea University, Seoul 136-701, Korea.

[‡]Department of Chemical and Biological Engineering, Korea University, Seoul 136-713, Korea

[§]Multidimensional Spectroscopy Laboratory, Korea Basic Science Institute, Seoul 136-713, Korea.

Supporting Information

ABSTRACT: Spectroscopic properties (i.e., peak positions and widths) of vibrational probes are sensitively dependent on their local environments in liquids. Such spectroscopic sensitivities can be utilized for studying the structures and dynamics of a variety of molecular systems. Here, we have studied the ion pairing equilibrium and dynamics of $SeCN^-$ ion pairs with Li^+ and Mg^{2+} cations in *N,N*-dimethylformamide (DMF). $SeCN^-$ ion is an excellent vibrational probe for studying ion dynamics in electrolyte solutions, not only because the vibrational lifetime of the CN stretch is substantially long but also because the CN stretch frequency is very sensitive to its local environment. When $SeCN^-$ ion forms contact ion pairs (CIPs) with Li^+ (Mg^{2+}) ion in DMF solutions, the CN stretch frequency is found to be significantly blue-shifted such that free $SeCN^-$ ion is spectrally well distinguished from Li-SeCN CIP and Mg-$SeCN^+$ CIP. This fact allows us to study the ion pairing equilibrium between $SeCN^-$ ion and metal ions as well as the dynamics of metal–$SeCN^-$ ion pairs. Ion pairing equilibrium between $SeCN^-$ ion and Li^+ (or Mg^{2+}) was studied by temperature-dependent Fourier transform infrared (FTIR) spectroscopy. The formation of CIPs in DMF was found to be entropically favored. Time-resolved IR pump–probe spectroscopy was used to study the vibrational population relaxation and orientational relaxation dynamics. Vibrational lifetimes of free $SeCN^-$ ion, Li-SeCN CIP, and Mg-$SeCN^+$ CIP were determined to be 83.6, 72.3, and 55.6 ps, respectively. Orientational relaxation dynamics were found to get slower in the order free $SeCN^-$ ion, Li-SeCN CIP, and Mg-$SeCN^+$ CIP. The orientational anisotropy decays of the CIPs, which were well fit by a biexponential function, were explained by two orientational relaxation processes, that is, a restricted (tethered) orientational relaxation of $SeCN^-$ within the CIPs followed by the overall orientational diffusion of the whole CIPs. The orientational relaxation time constants of Li-SeCN CIP and Mg-$SeCN^+$ CIP in DMF were twice different but the orientational diffusion radii calculated by the Debye–Stokes–Einstein equation were found to be almost identical within experimental error. The biexponential decay of the orientational anisotropy was analyzed by the wobbling-in-a-cone model. As a vibrational probe, $SeCN^-$ ion and SeCN group can be potentially used for measuring the molecular dynamics on a relatively long time scale because of their long lifetimes.

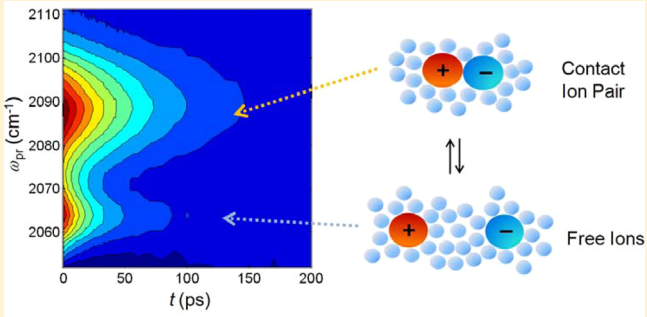

I. INTRODUCTION

Ions are involved in various chemical, physical, and biological processes in solutions.[1,2] In aqueous ionic solutions, dissolved ions perturb the hydrogen-bond network of water and thereby the dynamics of water are substantially changed.[3−5] The effects of ions on the structure and dynamics of water have been extensively studied by various experimental and theoretical methods.[3,4,6−10] Dissolved ions in protein solutions are well-known to disturb the tertiary structures of the proteins by directly interacting with the charged groups or polar groups of proteins.[2,11,12] Positive (negative) ions can associate with the negatively (positively) charged groups of the proteins by significantly perturbing the intramolecular interactions of the proteins. Understanding how the dissolved ions interact with the charged groups or polar groups of the proteins can be crucial to elucidate the effect of ions on the tertiary structures and the malfunctions of the proteins as well as the folding and unfolding dynamics of proteins. In highly concentrated electrolyte solutions, oppositely charged ions can associate to form ion pairs, and the ion pairs dissociate into free ions.[13−17] Such ion pairing equilibrium and dynamics play an important role in determining the physical properties of the electrolyte solutions.[1,18] To study the structures and dynamics of electrolyte solutions, a variety of experimental methods, such as conductometry,[19,20] dielectric relaxation spectroscopy,[21,22] ultrasonic relaxation,[23] temperature-jump relaxation,[24] and other spectroscopic methods[25−27] have been extensively used.

Received: May 11, 2012
Revised: June 29, 2012
Published: July 2, 2012

In the present work, we have studied the equilibrium and dynamics of ionic species in *N*,*N*-dimethylformamide (DMF) electrolyte solutions by Fourier transform infrared (FTIR) spectroscopy and IR pump−probe experiments. DMF is a polar organic solvent with a relatively high dielectric constant (ε_r = 36.7). Alkali metal ions and alkaline earth metal ions can be easily dissolved in DMF. At high ionic concentrations, Li^+ and $SeCN^-$ ions are found to associate to form Li-SeCN contact ion pairs (CIPs), and Mg^{2+} and $SeCN^-$ ions also associate to form Mg-$SeCN^+$ CIPs in DMF solution [to denote the contact ion pair (CIP), we use a dash between cation and $SeCN^-$ ion and the formal charge is added at the end). Temperature-dependent FTIR spectroscopy was used to determine the thermodynamic properties (ΔH and ΔS) of ion pairing equilibrium. Polarization-controlled IR pump−probe spectroscopy was used to investigate the vibrational population relaxation and orientational relaxation dynamics of free $SeCN^-$ ion, Li-SeCN CIP, and Mg-$SeCN^+$ CIP in DMF. Here, we used $SeCN^-$ ion as a vibrational probe because it has a long vibrational lifetime and its CN stretch is sensitively varied depending on its local environments. The CN stretch mode of $SeCN^-$ ion was peaked at ∼2066 cm^{-1} when it exists as a free ion in polar organic solvents. The CN stretch frequency of $SeCN^-$ ion is significantly blue-shifted when $SeCN^-$ ion forms the CIPs with dissolved cations. Therefore, IR spectroscopy can provide an opportunity to investigate the dynamics of free ions (FIs) and CIPs as well as the ion pairing equilibrium between the FIs and CIPs in electrolyte solutions. Time-resolved IR spectroscopy has advantages over conventional experimental methods (i.e., dielectric relaxation spectroscopy and conductometry) in directly measuring the dynamics of ionic species in electrolyte solutions occurring on picosecond time scales. Recently, vibrational population relaxation and orientational relaxation dynamics of ionic species in polar solvents were measured by IR pump−probe spectroscopy.[28−31] More recently, chemical exchange two-dimensional (2D) IR spectroscopy was employed to directly study ion pairing dynamics in real time.[32−34] These studies have demonstrated that ion dynamics in electrolyte solutions could be successfully investigated by probing molecular ions.

II. EXPERIMENTAL METHODS

A. Sample Preparation. Reagent-grade KSeCN, LiBr, and $Mg(ClO_4)_2$ were purchased from Sigma−Aldrich and were used without further purification. All sample solutions were prepared by directly dissolving salts in *N*,*N*-dimethylformamide (DMF). KSeCN salt was directly dissolved in DMF to prepare sample solutions, and 0.347 M KSeCN solution was used as a reference solution. Li^+ (from LiBr) and Mg^{2+} [from $Mg(ClO_4)_2$] ions were added to vary the molar ratio between cation and anion. In both electrolyte solutions, KBr or $KClO_4$ salts were precipitated due to their low solubility in DMF and were removed from the sample solutions by centrifugation.

B. Fourier Transform Infrared Spectroscopy. FTIR spectra were collected by using the Jasco FTIR spectrometer (FT/IR-4100) with 1 cm^{-1} resolution at 22 °C. The absorbance of sample solutions for all experiments was adjusted to be ∼0.2 at the peak. The sample solutions were housed in a homemade IR cell with two CaF_2 windows. The cell path length was varied by using a Teflon spacer of different thickness (6 or 12 μm).

Temperature-dependent FTIR spectra of both Li^+ + $SeCN^-$ ions and Mg^{2+} + $SeCN^-$ ions in DMF were measured from 30 to 80 °C at intervals of 10 °C. At each temperature, the cell was kept for at least 15 min before the FTIR spectrum was taken to make sure thermal equilibrium was reached. A temperature-controlled FTIR cell (Harrick) was used for the experiments. A temperature controller (Watlow) with a thermocouple (type K) inserted directly into the cell body was used to monitor and raise the temperature of the cell. In addition, the water bath was also connected with the cell body such that the water from the water bath was circulated through to stabilize and balance the temperature of the cell. The sample cell compartment in the FTIR spectrometer was continuously purged with dry air to remove water and CO_2 during the measurements.

C. Polarization-Controlled IR Pump−Probe Spectroscopy. The femtosecond laser system employed in our experiments has a similar design that has been described in detail elsewhere.[35,36] Briefly, a train of 800 nm pulses with ∼45 fs duration and ∼1.0 mJ/pulse was generated by a Ti:sapphire oscillator (Tsunami, Spectra-Physics) and regenerative amplifier (Spitfire, Spectra-Physics) laser system operating at 1 kHz. The 800 nm pulses were used to pump an optical parametric amplifier (OPA, Spectra-Physics) to produce near-IR pulses at ∼1.4 and ∼1.9 μm, which were used to generate mid-IR pulses at 2070 cm^{-1} in a 0.5 mm thick $AgGaS_2$ crystal by difference frequency generation. The power spectrum of the mid-IR pulses had a Gaussian envelope with a ∼260 cm^{-1} bandwidth (full width at half-maximum). CaF_2 plates with different thicknesses were used to compensate for the linear dispersion introduced by other dielectric materials in the setup, including a Ge Brewster plate and ZnSe beam splitters. The mid-IR pulses were nearly transform-limited at the sample position.

Experimental details of IR pump−probe spectroscopy have been described elsewhere.[4,37] The IR pulses from the laser system are split into the pump and probe beams and are focused onto the sample. The probe beam is collimated after the sample and is dispersed through a spectrometer onto the 64-element mercury−cadmium−telluride (MCT) array detector. The IR pump−probe signals were measured by setting the polarization of the probe beam parallel, $S_{\parallel}(t)$, and perpendicular, $S_{\perp}(t)$, with respect to that of the pump beam. The wire-grid polarizers are placed in the pump and probe beam pathways before the sample and their polarization states are set to be 0° and 45° with respect to the normal to the optical table, respectively. A wire-grid analyzer polarizer on a motorized rotational stage is placed after the sample, and the vertical and horizontal polarizations of the probe beam are selectively measured by setting the analyzer polarizer to be 0° and 90° by the computer-controlled motorized rotational stage. In the IR pump−probe experiments, the parallel, $S_{\parallel}(t)$, and perpendicular, $S_{\perp}(t)$, components of the pump−probe signals at each frequency are consecutively measured for every two scans with the polarization of the probe beam parallel and perpendicular to the pump beam, respectively.

III. RESULTS AND DISCUSSION

A. Fourier Transform Infrared Study. $SeCN^-$ ion is a linear triatomic molecule, has $C_{\infty v}$ symmetry, and has three IR-active vibrations: Se−C stretch (∼520 cm^{-1}), CN stretch (∼2070 cm^{-1}), and doubly degenerate bending of SeCN (∼400 cm^{-1}). Figure 1 displays the FTIR spectra of Li^+ + $SeCN^-$ ions and Mg^{2+} + $SeCN^-$ ions in DMF at different cationic concentrations. The CN stretch mode of free $SeCN^-$ ion is peaked at 2066 cm^{-1} in DMF. As the concentrations of Li^+ and Mg^{2+} ions are increased, the amplitude of the low-frequency peak gradually decreases but the amplitude of the high-frequency peak increases. The high-frequency peaks at 2080 cm^{-1} in Figure 1A result from the Li-SeCN CIP, while the high-frequency peak at

dx.doi.org/10.1021/jp304595n | J. Phys. Chem. B 2012, 116, 9152−9159

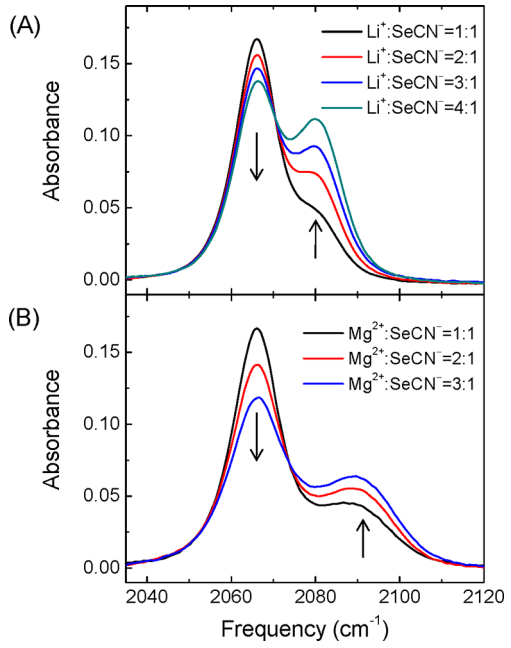

Figure 1. FTIR spectra of $MSeCN^{(n-1)+}$ (M = Li^+ or Mg^{2+}) at different cationic concentrations. [$SeCN^-$] = 0.347 M is fixed. (A) The concentration ratio between Li^+ and $SeCN^-$ ions varies from 1:1 to 4:1. (B) The concentration ratio between Mg^{2+} and $SeCN^-$ ions varies from 1:1 to 3:1. The change in peak amplitude is indicated by the arrows as the concentration of Li^+ or Mg^{2+} ion is increased.

2089 cm^{-1} in Figure 1B results from the Mg-$SeCN^+$ CIP. The amplitude of the CN stretch mode of the CIP is proportional to the concentration of the cation. The CN stretch frequency of Mg-$SeCN^+$ CIP is higher than that of Li-SeCN CIP. Electrostatic interaction between Mg^{2+} and $SeCN^-$ ion in the Mg-$SeCN^+$ CIP is substantially larger, and thus this results in the larger blue shift in the CN stretch frequency.[27] The frequency shift of the CN stretch mode upon formation of ion pair results originally from the vibrational Stark effect. The electric field of the cation has effects on the vibrational structure of $SeCN^-$ ion, leading to the blue shift of the CN stretch frequency. Both spectra have an isosbestic point near 2070 cm^{-1}. The isosbestic point is the wavelength at which the two absorbing chemical species in equilibrium have the same molar absorptivity. The presence of the isosbestic point indicates that two chemical species, which are spectrally well distinct, contribute to the absorption around the isosbestic point. In the present experiments, free $SeCN^-$ and CIPs coexist in each solution. It should be noted that when $SeCN^-$ ion forms a CIP with countercation, two CIP configurations are possible in DMF solutions: N-bound CIP and Se-bound CIP. Quantum chemistry calculations indicate that the CN stretch frequency of the Se-bound CIP is significantly blue-shifted when compared with those of free $SeCN^-$ ion and N-bound CIP.[33,34] Therefore, the high-frequency peaks shown in Figure 1 result from the Se-bound CIPs. For the remainder of the paper, the CIPs are referred to as the Se-bound CIPs.

The CN stretch bands in the FTIR spectra were decomposed into two contributions as shown in Figure 2. Two peaks associated with free ion (FI) and contact ion pair (CIP) were well fit by two Voigt profiles centered at 2066 cm^{-1} for free $SeCN^-$ ion and 2080 cm^{-1} for the Li-SeCN CIP, respectively, in Figure 2A (2089 cm^{-1} for the Mg-$SeCN^+$ CIP in Figure 2B). The peak of Mg-$SeCN^+$ CIP was found to be much broader than that of Li-SeCN CIP. It indicates that the Mg-$SeCN^+$ CIP is more

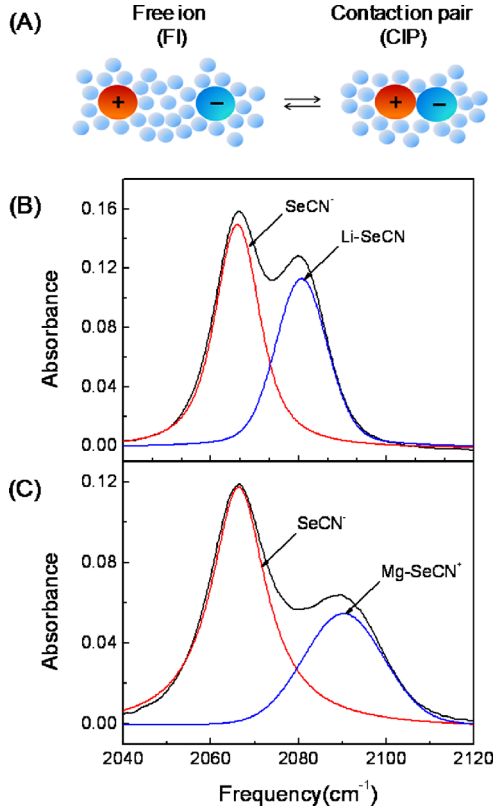

Figure 2. (A) Schematic illustration of ion pairing equilibrium in electrolyte solutions. (B) Decomposition of FTIR spectrum into free $SeCN^-$ ion and Li-SeCN CIP in DMF. (C) Decomposition of FTIR spectrum into free $SeCN^-$ ion and Mg-$SeCN^+$ CIP.

inhomogeneously distributed than the Li-SeCN CIP. The equilibrium between FI and CIP is written as

$$[M^{n+}] + [SeCN^-] \underset{k_d}{\overset{k_a}{\rightleftharpoons}} [M\text{-}SeCN^{(n-1)+}] \quad (1)$$

where k_a and k_d are the association and dissociation rate constant, respectively. If the activity coefficients are not taken into account, the equilibrium constant K_{eq} can be written as

$$K_{eq} = \frac{[M\text{-}SeCN^{(n-1)+}]}{[M^{n+}][SeCN^-]} = \frac{k_a}{k_d} \quad (2)$$

The concentrations of free $SeCN^-$ ion, Li^+ (Mg^{2+}), and Li-SeCN CIP (Mg-$SeCN^+$ CIP) are determined by the mass balances:

$$[SeCN^-]_0 = [SeCN^-] + [M\text{-}SeCN^{(n-1)+}] \quad (3)$$

$$[M^{n+}]_0 = [M^{n+}] + [M\text{-}SeCN^{(n-1)+}] \quad (4)$$

Once the concentrations of individual chemical species in each electrolyte solution are determined, the equilibrium constant can be calculated.

Figure 3 panels A and B display temperature-dependent FTIR spectra obtained with two electrolyte solutions. FTIR spectra were measured by increasing the temperature from 30 to 80 °C with an interval of 10 °C. In both electrolyte solutions, the amplitude of FI peak decreases gradually without significant change in its center frequency as the temperature is increased. On the other hand, the amplitude of CIP peak increases and its center frequency is red-shifted. This suggests that equilibrium shifts from the FI to the CIP configuration as the temperature is

dx.doi.org/10.1021/jp304595n | J. Phys. Chem. B 2012, 116, 9152–9159

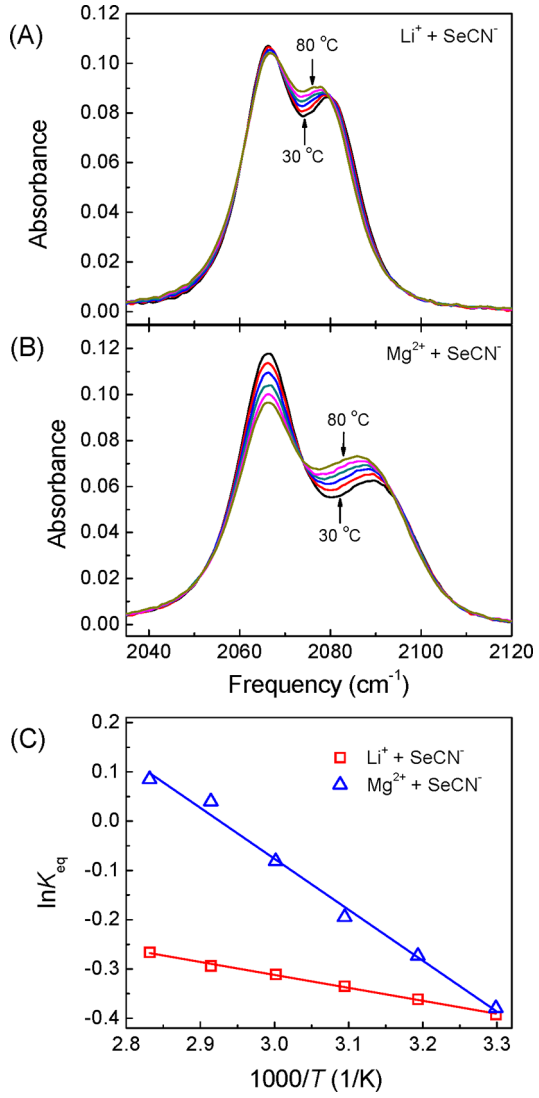

Figure 3. Temperature-dependent FTIR spectra measured with (A) Li^+ and $SeCN^-$ ions in DMF and (B) Mg^{2+} and $SeCN^-$ ions in DMF from 30 to 80 °C with an interval of 10 °C. (C) Temperature-dependent equilibrium constant (K_{eq}) of ion pairing equilibrium. The van't Hoff plot was used to determine the enthalpy and entropy of ion pairing equilibrium.

increased. The enthalpies and entropies of ion pairing equilibrium in both electrolyte solutions were obtained by using the van't Hoff plots as shown in Figure 3C and are summarized in Table 1.

Table 1. Enthalpies and Entropies of Ion Pairing Equilibrium

	ΔH(kJ/mol)	ΔS(J/K·mol)
Li-SeCN	2.18	3.96
Mg-$SeCN^+$	6.50	16.0

In Table 1, both ΔH and ΔS are positive for the formation of Li-SeCN CIP and Mg-$SeCN^+$ CIP. Positive enthalpy change (ΔH) indicates that both Li-SeCN CIP and Mg-$SeCN^+$ CIP formations are energetically unfavorable. In DMF solutions, the metal ion is solvated by DMF molecules. In order for the metal ion to form a CIP with $SeCN^-$, one of the solvated DMF molecules needs to be replaced by $SeCN^-$ ion. The positive ΔH indicates that the binding energy between the metal ion and DMF molecules is larger than that between the metal ion and $SeCN^-$ ion. On the other hand, both Li-SeCN CIP and Mg-$SeCN^+$ CIP formations are entropically favored. For a bimolecular recombination reaction in the gas phase, the entropy decreases. However, in solution, the solvent molecules around the solutes should be taken into account. When the CIP is formed, the solvent molecules are released from the solvation shells of the ions and their structures become more disordered. For two electrolyte solutions, the CIP formation is entropically more favored at higher temperatures.

B. Dispersive IR Pump–Probe Study. In IR pump–probe spectroscopy, the molecular system is vibrationally excited to $v = 1$ state by the IR pump beam. The subsequent relaxation of the vibrationally excited molecules is monitored by the time-delayed IR probe beam, which is frequency-resolved, giving the dispersive IR pump–probe signals. The transmission of the probe beam through the sample is measured with the pump beam on and off in the experiments. The IR pump–probe signals decay due to vibrational population relaxation and orientational relaxation. Accordingly, the parallel and perpendicular dispersive IR pump–probe signals measured in two-beam polarization geometries are written as[3,4]

$$S_{\parallel}(t, \omega_{pr}) = P(t, \omega_{pr})\left[1 + \frac{4}{5}C_2(t, \omega_{pr})\right] \quad (5)$$

$$S_{\perp}(t, \omega_{pr}) = P(t, \omega_{pr})\left[1 - \frac{2}{5}C_2(t, \omega_{pr})\right] \quad (6)$$

where $P(t,\omega_{pr})$ represents the vibrational population relaxation, and $C_2(t,\omega_{pr})$ is the orientational correlation function and is represented by the second-order Legendre polynomial of the transition dipole correlation function, $C_2(t) = \langle P_2[\boldsymbol{\mu}(t)\boldsymbol{\mu}(0)]\rangle$ at each probe frequency. Figure 4 displays the dispersive parallel and perpendicular IR pump–probe signals, $S_{\parallel}(t,\omega_{pr})$ and $S_{\perp}(t,\omega_{pr})$, obtained with LiSeCN and $MgSeCN^+$ sample solutions. The dispersive IR pump–probe signal is contributed by the ground-state bleach (GSB, $v = 0\rightarrow1$) and stimulated emission (SE, $v = 1\rightarrow0$) or the excited-state absorption (ESA, $v = 1\rightarrow2$). In Figure 4, the GSB and SE lead to an increase in the transmission of the probe beam (positive and shown in red), while the ESA results in the absorption of the probe beam (negative and shown in blue). In Figure 4, the contributions of free $SeCN^-$ ion and Li-SeCN CIP are observed to be spectrally well separated in the dispersive IR pump–probe signals obtained from Li^+ and $SeCN^-$ ions in DMF. In other words, two positive (red) peaks ($v = 0\rightarrow1$ and $v = 1\rightarrow0$) and two negative (blue) peaks ($v = 1\rightarrow2$) are well distinct in the dispersive IR pump–probe signals. However, in the case of Mg^{2+} and $SeCN^-$ ions in DMF, the positive signal from the fundamental transition of Mg-$SeCN^+$ CIP is substantially overlapped with the negative signal from the excited-state absorption of free $SeCN^-$ ion and they are partially canceled at around 2066 cm^{-1}. Therefore, the dispersive IR pump–probe signal obtained from Mg^{2+} and $SeCN^-$ ions in DMF appears to be different from that obtained from Li^+ and $SeCN^-$ ions in DMF.

1. Vibrational Population Relaxation Dynamics. The vibrational population relaxation decay, $P(t;\omega_{pr})$, at a given probe frequency (ω_{pr}) is obtained by using eqs 5 and 6:

$$P(t; \omega_{pr}) = S_{\parallel}(t; \omega_{pr}) + 2S_{\perp}(t; \omega_{pr}) \quad (7)$$

dx.doi.org/10.1021/jp304595n | J. Phys. Chem. B 2012, 116, 9152–9159

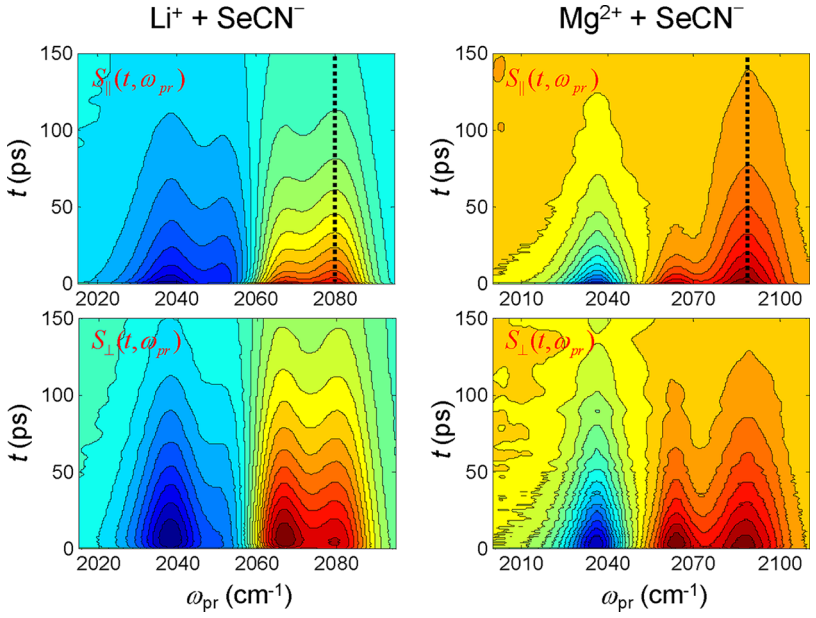

Figure 4. Parallel $[S_{\parallel}(t,\omega_{pr})$, upper panels] and perpendicular $[S_{\perp}(t,\omega_{pr})$, lower panels] dispersive IR pump−probe signals measured with Li^+ and $SeCN^-$ ions in DMF (left panels) and with Mg^{2+} and $SeCN^-$ ions in DMF (right panels). In the case of Mg^{2+} and $SeCN^-$ ions in DMF, the positive signal from the fundamental transition of Mg-$SeCN^+$ CIP is substantially overlapped with the negative signal from the excited-state absorption of free $SeCN^-$ ion.

Figure 5 displays the vibrational population relaxation decays of the CN stretch mode in free $SeCN^-$ ion, LiSeCN CIP, and Mg-$SeCN^+$ CIP at the fundamental ($v = 0 \leftrightarrow 1$) transition. $P(t;\omega_{pr})$ is directly proportional to the population of the vibrationally excited molecules at a given pump−probe delay time (t). Therefore, $P(t;\omega_{pr})$ is well described by a first-order kinetic process and is well fit by a single exponential function at a given probe frequency:

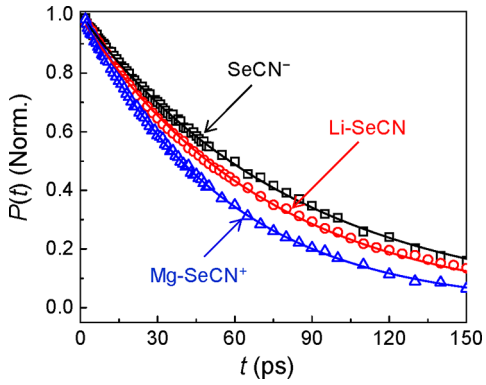

Figure 5. Vibrational population relaxation decays, $P(t)$, measured with free $SeCN^-$ ion, Li-SeCN CIP, and Mg-$SeCN^+$ CIP. Data points were experimentally measured. Solid lines are single exponential fits.

$$P(t;\ \omega_{pr}) = A\ \exp(-t/T_1) \tag{8}$$

where T_1 is the vibrational lifetime. The fit result is summarized in Table 2. As shown in Figure 5 and Table 2, the vibrational lifetimes of free $SeCN^-$ ion (T_1 = 83.6 ps), Li-SeCN CIP (T_1 = 72.3 ps), and Mg-$SeCN^+$ CIP (T_1 = 55.6 ps) in DMF are very long compared with those of other molecular ions, and they grow shorter in the order free $SeCN^-$ ion, Li-SeCN CIP, and Mg-$SeCN^+$ CIP. The population relaxation decay is relatively faster in the CIPs, indicating that the cations (Li^+ and Mg^{2+}) in the CIPs play an important role in providing additional vibrational relaxation pathways. In DMF solutions, the cations in the CIPs are also coordinated by the oxygen atom of DMF molecules. Intermolecular relaxation to DMF molecules through the cations might be more effective in the Li-SeCN CIP and Mg-$SeCN^+$ CIP than free $SeCN^-$ ions. Since vibrational population relaxation rate of a polyatomic molecule is influenced by many factors, it may not be clearly explained by a limited amount of experimental results. Recently, vibrational population relaxation of free OCN^-, SCN^-, and $SeCN^-$ ions in polar solvents were studied by Lian and co-workers.[30] They have shown that the vibrational lifetime of the CN stretch of free OCN^-, SCN^-, and $SeCN^-$ ion is solvent-dependent as a result of different intermolecular vibrational relaxation and generally grows longer in going from OCN^- to SCN^- to $SeCN^-$ ion, reflecting the effect of intramolecular vibrational relaxation.

2. Orientational Relaxation Dynamics. In IR pump−probe experiments, vibrational excitation of the molecular system by the linearly polarized pump pulse results in a $\cos^2\theta$ distribution of vibrationally excited molecules and the corresponding orientational holes in the ground-state distribution, where θ

Table 2. Exponential Fits to the Orientational Anisotropy and Population Relaxation

	ω_{pr} (cm^{-1})	a_1	τ_{or1} (ps)	a_2	τ_{or2} (ps)	T_1 (ps)
$SeCN^-$	2066	0.23 ± 0.01	2.7 ± 0.1	0.08 ± 0.01	16.8 ± 1.3	83.6 ± 0.3
Li-SeCN	2080	0.09 ± 0.01	8.1 ± 0.5	0.27 ± 0.01	129 ± 2	72.3 ± 0.3
Mg-$SeCN^+$	2089	0.07 ± 0.01	6.9 ± 0.8	0.29 ± 0.01	268 ± 11	55.6 ± 0.2

dx.doi.org/10.1021/jp304595n | J. Phys. Chem. B 2012, 116, 9152−9159

represents the angle between the transition dipole moment and the pump polarization vector. The transition dipoles of vibrationally excited molecules are randomized as the excited molecules undergo orientational relaxation. Therefore, the IR pump−probe signal includes information on the orientational relaxation dynamics of the probing molecule. The orientational anisotropy decay, $r(t,\omega_{pr})$, can be calculated from the parallel and perpendicular dispersive IR pump−probe signals:

$$r(t, \omega_{pr}) = \frac{S_{\parallel}(t, \omega_{pr}) - S_{\perp}(t, \omega_{pr})}{S_{\parallel}(t, \omega_{pr}) + 2S_{\perp}(t, \omega_{pr})} = \frac{2}{5}C_2(t, \omega_{pr}) \quad (9)$$

Figure 6A displays the orientational anisotropy decays of free $SeCN^-$ ion, Li-SeCN CIP, and Mg-$SeCN^+$ CIP in DMF. In fact,

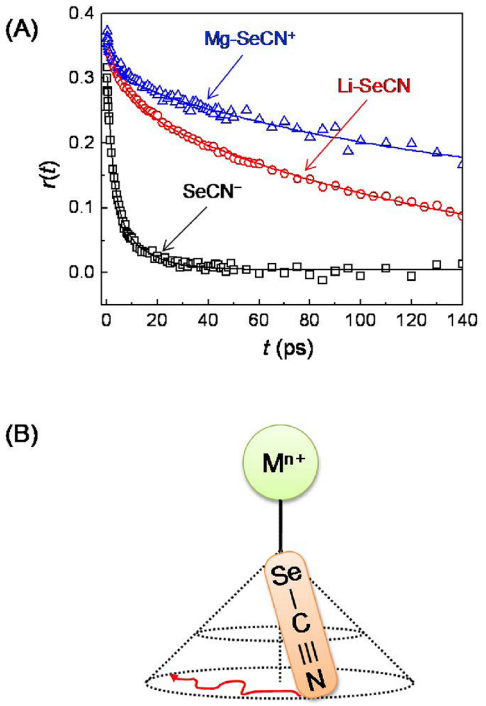

Figure 6. (A) Orientational anisotropy decays, $r(t)$, measured with free $SeCN^-$ ion, Li-SeCN CIP, and Mg-$SeCN^+$ CIP. Data points were experimentally measured. Solid lines are biexponential fits. (B) Schematic illustration of tethered orientational motion of $SeCN^-$ occurring at short times. $SeCN^-$ is coordinated to the metal ion, but its transition dipole can be randomized within the frame of the CIP.

the orientational anisotropy has a theoretical maximum value of 0.4 at $t = 0$ ps. However, the values of the orientational anisotropy experimentally determined at $t = 0$ ps are less than 0.4. This results from the fact that the measurement cannot fully resolve the initial inertial orientation relaxation dynamics of the probing molecules. The orientational anisotropy decays at a given probe frequency were well represented by a biexponential function:

$$r(t; \omega_{pr}) = a_1 \exp(-t/\tau_{or1}) + a_2 \exp(-t/\tau_{or2}) \quad (10)$$

where $\tau_{or1} < \tau_{or2}$. The biexponential fit result is summarized in Table 2. In the case of free $SeCN^-$ ion, the short time component (τ_{or1}) predominantly contributes to the orientational anisotropy decay. The biexponential decay of the orientational anisotropy of free $SeCN^-$ ion indicates that the orientational relaxation dynamics of free $SeCN^-$ ion deviate from simple hydrodynamic behaviors. This may result from the fact that (1) $SeCN^-$ ion is a linear molecular ion, (2) its size is comparable to that of the solvent molecule (DMF), and (3) the Se atom of $SeCN^-$ ion interacts with the hydrogen atom of DMF molecule by a relatively strong ion−dipole interaction (−CH···$SeCN^-$). Accordingly, the orientational relaxation of free $SeCN^-$ ion in DMF is restricted by the ion−dipole interaction between free $SeCN^-$ ion and DMF molecules.[4,37−41] The short time component of the orientational anisotropy decay of free $SeCN^-$ ion results from a restricted orientational diffusion of $SeCN^-$ ion due to the ion−dipole interaction, while the long time component is associated with the full diffusive orientational relaxation that is accompanied by breaking the ion−dipole interaction.

In the case of CIPs, the biexponential decay of the orientational anisotropy indicates that there are also two orientational relaxation processes that are temporally well distinct. The long time component (τ_{or2}) predominantly contributes to the orientational anisotropy decay of the CIPs. As shown in Table 2, the short time components of the orientational anisotropy decays are on a similar time scale for Li-SeCN and Mg-$SeCN^+$ CIPs, while the long time components are significantly different. In addition, the short time components of orientational anisotropy decays are independent of solution viscosity, while the long time components are strongly correlated with solution viscosity (see Table 3). As shown in Table 2, the

Table 3. Orientational Diffusion Radii of the CIPs Calculated from DSE Equation

	η^a (cP)	τ_{or2} (ps)	R (pm)
Li-SeCN	3.19 ± 0.5	129 ± 2	339 ± 30
Mg-$SeCN^+$	6.34 ± 0.2	268 ± 11	344 ± 20

[a] η was measured by the Ostwald viscometer.

long time component (τ_{or2}) of orientational anisotropy decay for the Mg-$SeCN^+$ CIP is twice as slow as that for the Li-SeCN CIP. The solution viscosity (η) shows the same trend in Table 3. It should be noted that ion pairing dynamics between Li^+ and $SeCN^-$ ions in DMF were investigated by chemical exchange 2D IR spectroscopy and the dissociation time constant of Li-SeCN CIP was found to be 620 ps.[33] The orientational relaxation time constant (129 ps) of Li-SeCN CIP was much shorter than the dissociation time constant, indicating that the orientational relaxation of Li-SeCN CIP is complete before the Li-SeCN CIP dissociates into Li^+ and $SeCN^-$ ions. Under the same experimental conditions, the dissociation of Mg-$SeCN^+$ CIPs would occur on a much longer time scale because the electrostatic interaction between Mg^{2+} and $SeCN^-$ ions is stronger. The short time component of the orientational anisotropy decay is attributed to the tethered orientational motion of $SeCN^-$ within the CIP as illustrated in Figure 6B, whereas the long time component results from the overall orientational motion of the whole CIPs. Here, the tethered orientational motion of $SeCN^-$ within the CIPs can be thought of as a local angular fluctuation of metal−$SeCN^-$ and should be less influenced by the solution viscosity. However, the overall orientational diffusion of the CIP should be dependent on the solution viscosity. The linear relationship between orientational relaxation time (τ_{or}) and solution viscosity (η) is given by the Debye−Stokes−Einstein (DSE) equation:[42,43]

$$\tau_{or} = \frac{\eta V}{k_B T} \quad (11)$$

dx.doi.org/10.1021/jp304595n | J. Phys. Chem. B 2012, 116, 9152−9159

where k_B and T are the Boltzmann constant and temperature, respectively, and V is the volume of the solute molecule. For spherically shaped solutes, $V = 4\pi R^3/3$ and thus the orientational diffusion radius (R) of the solute can be obtained by

$$R = \left(\frac{3k_BT}{4\pi}\frac{\tau_{or}}{\eta}\right)^{1/3} \quad (12)$$

If the solution viscosity (η) and the orientational relaxation time (τ_{or}) are experimentally determined, the orientational diffusion radius of the solute can be readily calculated. Here, we used the long time components of orientational anisotropy decays for the Li-SeCN and Mg-SeCN$^+$ CIPs to calculate the orientational diffusion radii (R) of the Li-SeCN and Mg-SeCN$^+$ CIPs in DMF solutions in Table 3. The solution viscosity was measured by the Ostwald viscometer. The orientational diffusion radii of Li-SeCN CIP and Mg-SeCN$^+$ CIP were calculated to be 339 ± 30 and 344 ± 20 pm, respectively, which are the same within experimental error. The orientational diffusion radius of free SeCN$^-$ ion in DMF was found to be approximately a factor of 2 smaller than that of the CIPs. This indicates that the orientational diffusion radii of the CIPs are considerably larger than what is predicted from the ionic radii. In addition, it was found from the quantum chemistry calculation that Li^+ and Mg^{2+} ions in the CIPs are also strongly coordinated by DMF molecules.[33] These results lead us to conclude that the overall orientational relaxation of the CIPs is accompanied by rotation of the coordinated DMF molecules.

In the context of a restricted orientational relaxation, the biexponential behaviors of the orientational anisotropy of free SeCN$^-$ ion, Li-SeCN CIP, and Mg-SeCN$^+$ CIP can be analyzed within an extended wobbling-in-a-cone model.[3,37,41,44] In the standard model, two independent orientational diffusion processes are proceeding simultaneously. The short time component describes the motion of a restricted rotor, whereby the transition dipole moment can only undergo orientational diffusion within a cone of semiangle θ_c. The long time component accounts for the slower overall orientational relaxation without any angular restriction that results in complete orientational randomization. In this model, the orientational correlation function is given by[40,41]

$$C_2(t) = [Q^2 + (1 - Q^2)\exp(-t/\tau_w)]\exp(-t/\tau_m) = \frac{5}{2}r(t) \quad (13)$$

where Q^2 is the generalized order parameter that describes the degree of restriction on the wobbling-in-a-cone orientational motion. Q^2 satisfies the condition $0 \le Q^2 \le 1$, where $Q^2 = 0$ describes unrestricted orientational motion and $Q^2 = 1$ is no wobbling-in-a-cone orientational motion. τ_w is the time constant that describes the wobbling motion. The time constant of the final full diffusive orientational relaxation is denoted τ_m, which is equal to the long time constant in eq 10, $\tau_m = \tau_{or2}$. τ_m gives directly the orientational diffusion coefficient of the angularly unrestricted orientational relaxation from the relation between the decay of the second Legendre polynomial and the diffusion constant, $D_m = 1/6\tau_m$. τ_w is obtained from the experimentally measured τ_{or1} and τ_{or2} by the relationship $\tau_w = (\tau_{or1}^{-1} - \tau_{or2}^{-1})^{-1}$. The cone semiangle θ_c is obtained from the order parameter $Q^2 = [0.5\cos\theta_c(1 + \cos\theta_c)]^2$.[40,41,44] The wobbling-in-a-cone diffusion constant D_w is calculated by[40,41]

$$D_w = \frac{x_w^2(1 + x_w)^2\{\ln[(1 + x_w)/2] + (1 - x_w)/2\}}{\tau_w(1 - Q^2)[2(x_w - 1)]} + \frac{(1 - x_w)(6 + 8x_w - x_w^2 - 12x_w^3 - 7x_w^4)}{24\tau_w(1 - Q^2)} \quad (14)$$

where $x_w = \cos\theta_c$. In the limit of $\theta_c = 180°$, there is no restriction to the orientational diffusion and $Q^2 = 0$ and $D_w = 1/6\tau_w$. Table 4 summarizes the parameters obtained from the wobbling-in-a-cone model. As expected, the cone semiangle of free SeCN$^-$ ion is quite large. The wobbling motions of SeCN$^-$ ion in both Li-SeCN CIP and Mg-SeCN$^+$ CIP are similar in terms of the cone semiangle and the wobbling time constant.

Table 4. Cone Semiangles and Orientational Diffusion Constants

	θ_c (deg)	τ_w (ps)	D_w^{-1} (ps)	D_m^{-1} (ps)
SeCN$^-$	55	3.2	16.5	101
Li-SeCN	29	8.6	127	774
Mg-SeCN$^+$	26	7.1	124	1608

It should be pointed out that there are subtle differences even though the orientational anisotropies of free SeCN$^-$ ion, Li-SeCN CIP, and Mg-SeCN$^+$ CIP are analyzed by the wobbling-in-a-cone model in the same manner. In the case of free SeCN$^-$ ion, the wobbling orientational relaxation of free SeCN$^-$ ion results from the ion−dipole interaction between SeCN$^-$ ion and DMF molecule, and the overall orientational relaxation at long times occurs by breaking the ion−dipole interaction. In contrast, the wobbling motion of SeCN$^-$ ion in the CIPs is a restricted orientational diffusion of SeCN$^-$ ion within the CIP frame while the long time component of the orientational anisotropy results from the overall orientational diffusion of the whole CIPs. This is because the dissociations of Li-SeCN and Mg-SeCN$^+$ CIPs occur on much longer time scales than their overall orientational motions.[33]

IV. SUMMARY AND CONCLUDING REMARKS

In the present work, we have studied ion pairing equilibrium between metal ions (Li^+ and Mg^{2+}) and SeCN$^-$ ion by FTIR spectroscopy and vibrational population relaxation and orientational relaxation dynamics of free SeCN$^-$ ion, Li-SeCN CIP, and Mg-SeCN$^+$ CIP by IR pump−probe spectroscopy. The CN stretch vibration of SeCN$^-$ ion is sensitively dependent on its local environment. The CN stretch frequency is significantly blue-shifted when SeCN$^-$ ion forms a CIP with a metal ion. As a result, Li-SeCN CIP and Mg-SeCN$^+$ CIP are spectrally well distinct from free SeCN$^-$ ion in DMF electrolyte solutions. Temperature-dependent FTIR study indicates that the formation of Li-SeCN CIP and Mg-SeCN$^+$ CIP is endothermic and entropically favored. The lifetime of the CN stretch vibration of free SeCN$^-$ ion is measured to be very long (T_1 = 83.6 ps). When SeCN$^-$ ion forms a CIP with Li^+ or Mg^{2+} ion, the vibrational lifetime grows shorter (T_1 = 72.3 ps for Li-SeCN CIP and T_1 = 55.6 ps for Mg-SeCN$^+$ CIP, respectively). The biexponential behaviors of the orientational anisotropy are analyzed by the wobbling-in-a-cone model: (1) the restricted (tethered) orientational diffusion of SeCN$^-$ within the CIPs at short times and (2) the overall orientational relaxation of the whole CIPs at long times. The long time component is found to be strongly correlated with solution viscosity (η). The orientational diffusion

dx.doi.org/10.1021/jp304595n | J. Phys. Chem. B 2012, 116, 9152−9159

radii of the CIPs are calculated with the DSE equation by using the experimentally measured τ_{or2} and η. The orientational diffusion radii of Li-SeCN CIP and Mg-$SeCN^+$ CIP are found to be the same within experimental error.

As mentioned in Introduction, the effects of ions are ubiquitous. However, ion dynamics have not been fully understood. This may result partially from the experimental difficulty in directly monitoring the ionic species or the effects of ions. A recent development of time-resolved IR spectroscopy has opened the door for investigating molecular dynamics by probing the molecular vibrations. As shown here, spectroscopic properties of a molecular ion (e.g., $SeCN^-$ ion) were sensitively varied depending on their local environments. The CN stretch frequency of $SeCN^-$ ion was found to depend linearly on the strength of ion−molecule interaction, allowing spectroscopic distinctions among different ionic configurations (i.e., free $SeCN^-$ ion, Li-SeCN CIP, and Mg-$SeCN^+$ CIP). Therefore, the dynamics of individual ionic species were able to be separately investigated. Moreover, the interconversion dynamics between them occurring under thermal equilibrium conditions can be studied if they occur on experimentally measurable time scales. In addition, the effect of ions on the structures and dynamics of proteins can be vibrationally probed. For example, if the amide groups of polypeptides are employed as IR probes, the interaction of dissolved ions with the backbone of polypeptides can be readily studied. IR probes such as SeCN, SCN, and N_3 group can be chemically introduced to the backbone of polypeptides to monitor the local structural changes of proteins.

In time-resolved IR experiments including IR pump−probe spectroscopy and 2D IR spectroscopy, the study of molecular dynamics by using IR probes is sometimes limited by the vibrational lifetimes of the IR probes because the time-resolved IR signal is directly proportional to the population on the vibrationally excited state. Once the vibrationally excited molecules relax back to the ground state, the signal cannot be measured. Therefore, vibrational probes with long lifetimes can extend our experimental time range for investigating molecular dynamics. In this sense, $SeCN^-$ ion can be an excellent vibrational probe for measuring molecular dynamics up to a few hundred picoseconds. In addition, it might be possible that the SeCN group can be introduced to the residues of proteins as a vibrational probe to study the conformational dynamics of proteins.

■ ASSOCIATED CONTENT

Ⓢ Supporting Information

One figure, showing parallel and perpendicular dispersive pump−probe signals measured with free $SeCN^-$ ions in DMF. This material is available free of charge via the Internet at http://pubs.acs.org.

■ AUTHOR INFORMATION

Corresponding Author

*E-mail spark8@korea.ac.kr.

Notes

The authors declare no competing financial interest.

■ ACKNOWLEDGMENTS

This work was supported by NRF grants (2010-0005020 and 2011-0002122) to S.P. This work was also supported by a Human Resources Development of the KETEP grant (20104010100640) to S.P.

■ REFERENCES

(1) Marcus, Y.; Hefter, G. *Chem. Rev.* **2006**, *106*, 4585.
(2) Nostro, P. L.; Ninham, B. W. *Chem. Rev.* **2012**, *112*, 2286.
(3) Park, S.; Fayer, M. D. *Proc. Natl. Acad. Sci. U.S.A.* **2007**, *104*, 16731.
(4) Park, S.; Moilanen, D. E.; Fayer, M. D. *J. Phys. Chem. B* **2008**, *102*, 5279.
(5) Asbury, J. B.; Steinel, T.; Kwak, K.; Corcelli, S. A.; Lawrence, C. P.; Skinner, J. L.; Fayer, M. D. *J. Chem. Phys.* **2004**, *121*, 12431.
(6) Laage, D.; Hynes, J. T. *Science* **2006**, *311*, 832.
(7) Park, S.; Odelius, M.; Gaffney, K. J. *J. Phys. Chem. B* **2009**, *113*, 7825.
(8) Tielrooij, K. J.; Garcia-Araez, N.; Bonn, M.; Bakker, H. J. *Science* **2010**, *328*, 1006.
(9) Fayer, M. D. *Acc. Chem. Res.* **2012**, *45*, 3.
(10) Lin, Y.-S.; Auer, B. M.; Skinner, J. L. *J. Chem. Phys.* **2009**, *131*, No. 144511.
(11) Collins, K. D. *Methods* **2004**, *34*, 300.
(12) Zhang, Y.; Cremer, P. S. *Curr. Opin, Chem. Biol.* **2006**, *10*, 658.
(13) Barthel, J.; Buchner, R.; Eberspächer, P.-N.; Münsterer, M.; Stauber, J.; Wurm, B. *J. Mol. Liq.* **1998**, *78*, 83.
(14) Kaatze, U.; Hushcha, T. O.; Eggers, F. *J. Solution Chem.* **2000**, *29*, 299.
(15) Buchner, R.; Samani, F.; May, P. M.; Sturm, P.; Hefter, G. *ChemPhysChem* **2003**, *4*, 373.
(16) Akilan, C.; Rohman, N.; Hefter, G.; Buchner, R. *ChemPhysChem* **2006**, *7*, 2319.
(17) Wachter, W.; Fernandez, S.; Buchner, R.; Hefter, G. *J. Phys. Chem. B* **2007**, *111*, 9010.
(18) Marcus, Y. *Ion Solvation*; Wiley: New York, 1985.
(19) Tomšič, M.; Bešter-Rogač, M.; Jamnik, A.; Neueder, R.; Barthel, J. *J. Solution Chem.* **2002**, *31*, 19.
(20) Jaipal Reddy, M.; Chu, P. P. *J. Power Sources* **2002**, *109*, 340.
(21) Buchner, R.; Hefter, G. T.; May, P. M. *J. Phys. Chem. A* **1998**, *103*, 1.
(22) Wurm, B.; Münsterer, M.; Richardi, J.; Buchner, R.; Barthel, J. *J. Mol. Liq.* **2005**, *119*, 97.
(23) Kaatze, U.; H., T. O.; Eggers, F. *J. Solution Chem.* **2000**, *29*, 299.
(24) Eigen, M.; Eyring, E. M. *J. Am. Chem. Soc.* **1962**, *84*, 3254.
(25) Le Borgne, C.; Illien, B.; Beignon, M.; Chabanel, M. *Phys. Chem. Chem. Phys.* **1999**, *1*, 4701.
(26) Barthel, J.; Buchner, R.; Wismeth, E. *J. Solution Chem.* **2000**, *29*, 937.
(27) Le Borgne, C.; Chabanel, M. *J. Mol. Liq.* **1997**, *73*−*74*, 171.
(28) Zhong, Q.; Owrutsky, J. C. *Chem. Phys. Lett.* **2004**, *383*, 176.
(29) Ohta, K.; Tominaga, K. *Chem. Phys. Lett.* **2006**, *429*, 136.
(30) Lenchenkov, V.; She, C.; Lian, T. *J. Phys. Chem. B* **2006**, *110*, 19990.
(31) Owrutsky, J. C.; Pomfret, M. B.; Barton, D. J.; Kidwell, D. A. *J. Chem. Phys.* **2008**, *129*, No. 024513.
(32) Park, S.; Ji, M.; Gaffney, K. J. *J. Phys. Chem. B* **2010**, *114*, 6693.
(33) Park, K.-H.; Choi, S. R.; Choi, J.-H.; Park, S.; Cho, M. *ChemPhysChem* **2010**, *11*, 3632.
(34) Lee, K.-K.; Park, K.-H.; Kwon, D.; Choi, J.-H.; Son, H.; Park, S.; Cho, M. *J. Chem. Phys.* **2011**, *134*, No. 064506.
(35) Park, S.; Kwak, K.; Fayer, M. D. *Laser Phys. Lett.* **2007**, *4*, 704.
(36) Lee, K.-K.; Park, K.-H.; Choi, J.-H.; Ha, J.-H.; Jeon, S.-J.; Cho, M. *J. Phys. Chem. A* **2010**, *114*, 2757.
(37) Moilanen, D. E.; Piletic, I. R.; Fayer, M. D. *J. Phys. Chem. C* **2007**, *111*, 8884.
(38) Wang, C. C.; Pecora, R. *J. Chem. Phys.* **1980**, *72*, 5333.
(39) Kinosita, K.; Ikegami, A.; Kawato, S. *Biophys. J.* **1982**, *37*, 461.
(40) Lipari, G.; Szabo, A. *Biophys. J.* **1980**, *30*, 489.
(41) Tan, H.-S.; Piletic, I. R.; Fayer, M. D. *J. Chem. Phys.* **2005**, *122*, No. 174501.
(42) Köddermann, T.; Ludwig, R.; Paschek, D. *ChemPhysChem* **2008**, *9*, 1851.
(43) Hagopian, S.; Whittenburg, S. L. *J. Mol. Liq.* **1990**, *45*, 273.
(44) Gaffney, K. J.; Piletic, I. R.; Fayer, M. D. *J. Chem. Phys.* **2003**, *118*, 2270.